Received: 17 September 2023 | Revised: 20 October 2023 | Accepted: 30 October 2023
DOI: 10.1002/nano.202300140

REVIEW

Recent advances in TiO_2 nanotube layers – A mini review of the latest developments in nanotube preparation and applications in photocatalysis and microwave sensing

Hanna Sopha[1,2] | **Mahnaz Alijani**[2] | **Marcela Sepúlveda**[1] | **Jan M. Macak**[1,2]

[1]Center of Materials and Nanotechnologies, Faculty of Chemical Technology, University of Pardubice, Pardubice, Czech Republic
[2]Central European Institute of Technology, Brno University of Technology, Brno, Czech Republic

Correspondence
Hanna Sopha, Center of Materials and Nanotechnologies, Faculty of Chemical Technology, University of Pardubice, 53002 Pardubice, Czech Republic.
Email: hannaingrid.sopha@upce.cz

Funding information
Ministerstvo Školství, Mládeže a Tělovýchovy, Grant/Award Number: LM2023037

Abstract
Self-organized anodic TiO_2 nanotube (TNT) layers prepared by anodization of Ti substrates have attracted great interest within the last 20 years, due to their unique properties and low-cost synthesis. This mini review article aims to shortly summarize the most recent developments in the TNT layer synthesis and applications. It presents the synthesis of high aspect ratio (HAR) TNT layers in a short time by accelerating the TNT layer growth rates in lactic acid containing electrolytes. Furthermore, the etching of TNT layers towards TNT bundles of homogeneous size and single tube powders is discussed, as well as the possibility to grow TNT layers on non-planar Ti substrates, which cannot be directly connected to the potentiostat (e.g., Ti spheres or 3D Ti meshes). As a relatively new application, the employment of TNT layers in microwave resonator sensors is introduced. Last, but not least, approaches of upscaling the TNT layer size from the laboratory scale towards significantly larger scale are outlined and reviewed.

KEYWORDS
anodization, bipolar electrochemistry, etching, microwave resistor sensors, single nanotube powders, TiO_2 nanotube layers, upscaling

1 | INTRODUCTION

Since the first report in 1972 on the use of TiO_2 for photocatalytic water splitting by Fujishima and Honda,[1] TiO_2 gained high scientific and technological interests due to its possible employment in a plethora of applications, including photocatalysis,[2] solar energy conversion,[3] sensors,[4] or biomedicine (e.g., as implants).[5] The reason for the use of TiO_2 in these applications is related to its beneficial chemical and physical properties: its wide band gap (between 3.0 eV for rutile and 3.2 eV for anatase phase), its good ion intercalation and its biocompatibility.[5–8]

Nanostructured TiO_2 is of special significance as it provides extremely high surface area and many active sites. It is therefore not surprising that over the last decades extensive research efforts have been carried out to produce nanostructured TiO_2 in different shapes, as, for instance, nanoparticles,[9] nanorods,[10] nanofibres,[11] or nanotubes.[12,13] The most widely used TiO_2 nanostructures up to today are industrially produced nanoparticles, which can be found, for example, in sunscreen, paint, self-cleaning windows, or solar cells.

However, due to their hollow structure resulting in an enormous available surface area, TiO_2 nanotubes belong to the most interesting shapes and can be produced via different approaches, such as hydrothermal methods,[14] template assisted approaches,[15] electrospinning,[16] and anodization.[13,17] Most approaches result in the formation of nanotube powders, however, by anodization continuous TiO_2 nanotube (TNT) layers can be produced, which are directly connected to the anodized Ti substrates. Such TNT layers consist of vertically aligned nanotubes with strong interconnections and are highly self-ordered, which leads to an uni-directional charge transport along one direction (i.e., the nanotube walls) and therefore improved charge separation, as well as to directional diffusion profiles.[18] Due to the connection to the underlying Ti substrate, no additional immobilization of nanotubes is required for their further application.

Within the last 15 years, various review articles summarized the newest advancements in the field of TNT layers at the time of the publication; the first one published in 2007, reviewing the early research efforts, TNT layer properties and their applications.[19] In 2014, Lee et al. summarized practically all work carried out on TNT layers until then in an exhaustive review article.[20] Additionally, several smaller review articles were published on rather recent developments in the field being focused on special topics, such as the nanotube formation mechanism and nanotube structure[21–28] or nanotube functionalization,[29] or certain applications as for instance photocatalysis,[30] photoelectrocatalysis,[31] energy storage,[32–34] solar energy conversion,[35,36] biomedical applications,[37–40] supercapacitors,[41] or sensors.[42]

This mini review aims to give a brief overview on the most recent research efforts, new synthesis methods and applications raised within the last 3 to 5 years. This includes the synthesis of high aspect ratio TNT layers in a very short time, the use of bipolar electrochemistry to produce TNT layers on non-planar Ti objects, which cannot be connected directly to the potentiostat, and etching of TNT layers to single tube powders for an even increased surface area. Furthermore, the application of TNT layers in microwave sensors as a recent application will be discussed. Finally, upscaling of the TNT layers from the laboratory scale to large- or full-scale synthesis will be discussed, paving the way for industrial production of TNT layers for their commercial employment in conventional photocatalytic and other applications. Though also many other interesting studies were carried out within the last ~3–5 years for the use of TNT layers in different application, for instance on further improvement on photoelectrocatalysis (PEC)[43–46] or Li-ion batteries,[47–50] deeper investigations on cell response on TNT layers, [51–54] or the use of TNT layers as ion sieves for Li extraction,[55] this review does not focus on these applications. The reason is that many other recently published review articles, as mentioned above, are focused on them.

1.1 | High aspect ratio TiO_2 nanotube layers

While the first publication on TNT layers dates back to 1984,[12] enormous research efforts on their development were carried out in the early 2000s. In this time, special attention was drawn to the optimization of the electrolyte composition and especially towards the thickening TNT layers, as it was foreseen that this leads to a boosting of their performance. As a result, anodization electrolytes are nowadays classified into three different generations: (i) aqueous, acidic electrolytes, in which TNT layers with a thickness of up to ~500 nm can be prepared,[56,57] (ii) aqueous, neutral electrolytes, in which TNT layers with thickness up to ~4 µm can be prepared,[58–60] and (iii) organic viscous electrolytes (usually glycerol- or ethylene glycol-based), in which TNT layers with a thickness of several hundreds of µm can be prepared.[17,61–63] All electrolyte generations have the addition of small amounts of a F^- source in common, most frequently in the form of NH_4F or HF.[19,62]

Nowadays, the most commonly used electrolytes are based on ethylene glycol and glycerol, as thicker TNT layers exhibit higher surface area, which is advantageous for many applications.[62,64–68] The reason why thicker TNT layers can be received in ethylene glycol- and glycerol-based electrolytes compared to their aqueous counterparts, is the lower TiO_2 dissolution (etching) rate on their tops in these electrolytes as local concentration and pH fluctuations are suppressed due to the high viscosity.[61] However, the TiO_2 dissolution in these electrolytes is not only reduced on the nanotube tops but also on their bottoms, which means that long anodization times are required to receive thick TNT layers with a high aspect ratio (HAR), meaning the ratio between the nanotube layer thickness and the nanotube diameter. Depending on the final thickness of the TNT layers, the anodization time may take between several hours and several days.[61–63,68,69] Such long anodization times are neither economical nor environmentally friendly and must, therefore, be significantly reduced, to make the anodization process useful for industrial applications.

The path to receive HAR TNT layers within a reasonable time is obviously to increase their growth rate, which can be solved by increasing the anodization potential (or in the case of galvanostatic anodization the anodization current density). Nonetheless, this approach is not as straight forward as it appears on the first glance, as a higher electric field promotes the occurrence of dielectric breakdown, resulting in a "burning" of the Ti substrate by locally significantly increased current densities and temperatures, hampering the TNT layer synthesis.[70] The dielectric breakdown is an autocatalytic, avalanche reaction, triggered by the injection and further multiplication of electrons from the electrolyte species into the oxide conduction band.[71,72] Therefore, once the dielectric breakdown commenced, it cannot be stopped. Consequently, the anodization conditions must be carefully adjusted and optimized to receive high TNT layer growth rates without the occurrence of dielectric breakdown. This can for instance be achieved by further optimizing the anodization electrolyte by adding surfactants.

One of the first reports on the increase of the TNT layer growth rate investigated the addition of H_2O_2 to the electrolyte.[73] The H_2O_2 accelerated the growth rate, which was attributed to the formation of HO• and HO_2• radicals controlling the oxidation and dissolution processes. However, due to the short lifetime of H_2O_2, the growth rate increased just for a short time at the beginning of the anodization and slowed down in the frame of time.[73]

On the other hand, it is known that the breakdown potentials can be shifted towards higher potentials by the addition of weak chelating organic acids into the electrolyte.[65] The accelerated growth rate was first shown by Banerjee et al. for the use of the disodium salt of ethylene diaminetetraacetic acid ($Na_2[H_2EDTA]$), as addition to an ethylene glycol-based electrolyte, resulting in ~41 μm thick TNT layers produced within 1 hour of anodization.[74] Deeper investigations on the addition of other chelating agents, that is, lactic acid (LA), citric acid, glycolic acid, and EDTA, were further carried out by So et al.[65] It was found that the highest TNT layer growth rates were obtained upon the addition of LA. The addition of LA allowed to apply a potential about twice as high as in an LA-free electrolyte, without the risk of dielectric breakdown. Detailed x-ray Photoelectron Spectroscopy (XPS) and Time of Flight-Secondary Ion Mass Spectroscopy (ToF-SIMS) investigations confirmed the adsorption of LA from the electrolyte on the TiO_2 surface, preventing the dielectric breakdown during the anodization process. By employing an anodization potential of 120 V and additionally increasing the electrolyte temperature to 60°C, TNT layers with a thickness of ~150 μm were achieved within only 1 hour of anodization.[65] Furthermore, it must be noted that the TNT layers of 15 and 30 μm thickness, obtained on LA-containing electrolytes within only a few minutes, showed a significantly enhanced adherence to the underlying Ti substrate upon annealing compared to the TNT layers of similar thickness prepared in an LA-free electrolyte.[66]

To avoid the uneconomical and energy consuming heating of the electrolyte, Alijani et al. recently optimized the LA-containing electrolyte further.[75,76] It was shown that the aging of the electrolyte plays a significant role to receive HAR TNT layers within a very short time. Similarly, as for anodization in LA-free electrolytes,[77] LA containing electrolytes need to be aged. With aging the anodization of dummy Ti substrates is meant, which are not further used. By doing this, the electrolyte composition slightly changes by the electrode reactions. This results in the presence of Ti-F species (e.g., $[TiF_6]^{2-}$), therefore a small decrease in free F^- ions, and a slight increase in the H_2O concentration in the electrolyte. An additional use of the electrolyte, especially for short times, does not result in significant electrolyte changes afterwards for a certain time of electrolyte use.[77] By optimizing the electrolyte age, TNT layers with a thickness of ~80 μm could be obtained within 15 and 30 minutes by applying anodization potentials of 160 and 140 V, respectively.[75] By using galvanostatic anodization and applying a current density of 55 mA cm^{-2}, a TNT layer thickness of ~44 μm could be reached within 15 minutes.[76] It is important to note that no additional tedious heating or cooling of the electrolyte was employed in these studies.[75]

Overall, these most recent studies show the possibility of producing thick HAR TNT layers with AR up to ~450 in a reasonable short time of 30 minutes,[75,76] making the process economically realistic for a possible industrial application. Figure 1 gives an overview on AR and growth rate of TNT layers received in the different aqueous (a) and viscous (b) electrolytes.

1.2 | Etching of TiO_2 nanotube layers towards nanotube bundles and single tube powders

As described in Chapter 1.1, nowadays ethylene glycol and glycerol-based electrolytes with low water content are most commonly used to receive thick TNT layers. However, it was found that in such electrolytes nanotubes with a double wall (DW) structure are produced.[79,80] Figure 2 shows a scheme and a Scanning Electron Microscope (SEM) image of the DW structure after annealing treatment at 400°C at the bottom of a TNT layer prepared in an ethylene glycol-based electrolyte containing 150 mM NH_4F and 10 vol% H_2O. As during anodization a chemical etching takes place on the top of the TNT layers, the DW structure is not visible at the top of the layers. Furthermore, it becomes thicker towards the bottom of the TNT layers, forming a V-shape.[79]

DW TNT layers consist of two distinctly different regions: an outer shell (OS) and an inner shell (IS) of the

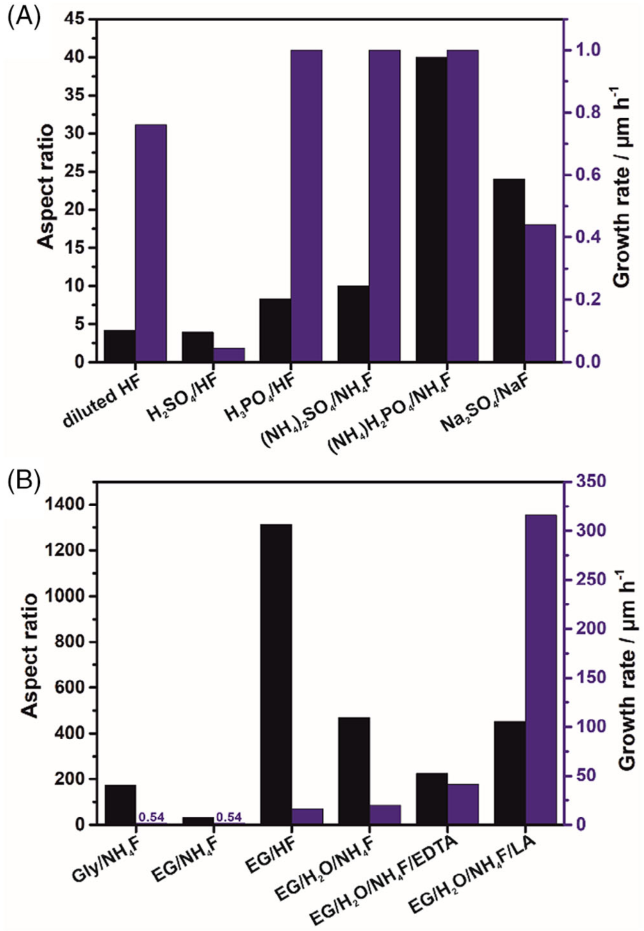

FIGURE 1 Aspect ratio and growth rate of TNT layers produced in (A) aqueous electrolytes (aqueous acidic electrolytes: diluted HF,[57] H_2SO_4/HF,[56] H_3PO_4/HF,[78] and aqueous neutral electrolytes: $(NH_4)_2SO_4/NH_4F$,[58] $(NH_4)H_2PO_4/NH_4F$,[60] Na_2SO_4/NaF),[59] and (B) organic viscous electrolytes (Gly/NH_4F,[61] EG/NH_4F,[17] EG/HF,[62] EG/H_2O/NH_4F,[77] EG/H_2O/NH_4F/EDTA,[74] EG/H_2O/NH_4F/LA).[75] Gly = glycerol, EG = ethylene glycol. TNT, TiO2 nanotube.

nanotubes. The reason for this can be explained by the TNT layer formation mechanism[81] and was in detail described in a recent book chapter.[23] In brief, during anodization the TiO_2 formation takes place on the metal-metal oxide as well as on the metal oxide-electrolyte interface. Simultaneously ethylene glycol or glycerol decompose in the high electrical field, applied for anodization. Thus, C-species from the decomposition are adsorbed on the metal oxide-electrolyte interface and consequently incorporated into the newly formed metal oxide. On the metal-metal oxide interface rather pure TiO_2 is formed. Considering the plastic flow model for the TNT layer formation,[81,82] the formed TiO_2 layer moves upwards with the pure TiO_2 layer, which was formed at the metal-metal oxide interface, building the OS of the formed nanotubes. The C-species rich layer, formed at the metal oxide-electrolyte interface, builds the IS. The enrichment of C-species from the electrolyte within the IS of the DW TNT layers was proven by two studies, deeply investigating the composition of the DW TNT layers.[83,84] The OS on the other hand was found of almost pure TiO_2, while F-species stemming from the electrolyte were mainly found between the individual nanotubes and between the TNT layer and the underlying Ti substrate.[83,84]

An pioneering study revealed that in comparison to single wall (SW) TNT layers (prepared in a dimethyl sulfoxide (DMSO)-based electrolyte), the DW TNT layers prepared in ethylene glycol-based electrolytes show a lower performance, as conductivity or electron transport times in DSSCs, layers as the carbon-containing IS has a negative influence on the charge recombination.[85] However, TNT layers grow extremely slow in DMSO.[81,85,86] Furthermore, TNT layers produced in ethylene glycol-based electrolytes are more homogeneous and of higher order,[86,87] and therefore the ethylene glycol-based electrolytes are still the most common.

Therefore, a chemical treatment of TNT layers prepared in ethylene glycol-based electrolytes was suggested, allowing the selective dissolution of the IS. As a result, SW TNT layers can be obtained.[88–92] This etching is carried out in piranha solution at elevated temperature after a mild pre-annealing at low temperatures of the TNT layers. A scheme and a SEM image of such a SW TNT layer obtained after chemical etching is shown in Figure 2.

As a consequence of the removal of the IS, SW TNT layers possess enhanced properties such as conductivity, carrier transport and a lower on-set temperature during annealing, due to the lower amount of impurities.[90,93,94] This results in improved photoelectrochemical and photocatalytic performances, compared to the DW ones.[88,90,92,95] Recently it was shown that a further reconstruction of the SW TNT layers by a thin TiO_2 coating, obtained by Atomic Layer Deposition (ALD) additionally improved the photoelectrochemical performance and photocatalytic activity of the SW TNT layers by a passivation of surface states within the TNT layers and an enhanced utilization of photogenerated charge carriers.[96]

By optimizing the etching process for SW TNT layers and, in particular, applying a prolonged ultrasonication step, the DW TNT layers can be etched to powders of TNT bundles. This process can be used to obtain TNT bundles of more homogenous size than obtained by bending of the Ti substrates. Figure 2 shows the scheme and a SEM image of TNT bundles obtained by etching of TNT layers. Furthermore, the C-rich IS should be removed from this TNT bundles. The application of such TNT bundles of more homogenous size was shown for photocatalytic active microrobots used for biofilm removal.[97] An

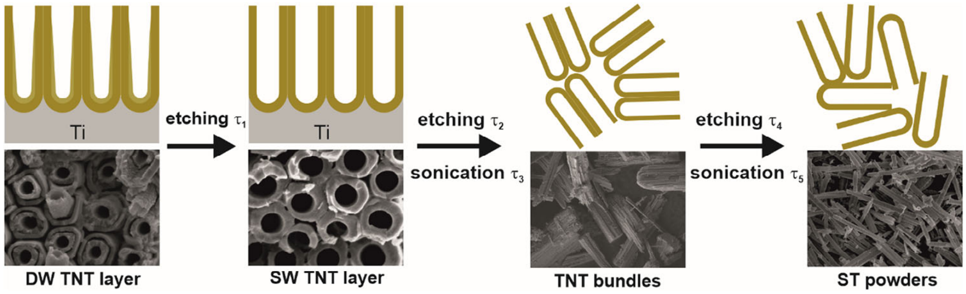

FIGURE 2 Scheme of different morphologies of TiO_2 nanotubes received via etching of DW TNT layers and corresponding SEM images revealing the real morphology: DW TNT layer, (Scanning Electron Microscope (SEM) image taken from the TNT layer bottom part), SW TNT layer after chemical etching time t_1 (SEM image taken from the TNT layer bottom), TNT bundles received after chemical etching time t_2 and sonication time t_3, and TiO_2 single tube powders received after chemical etching time t_4 and sonication time t_5. TNT, TiO_2 nanotube.

additional decoration of the TNT bundles with CdS using a hydrothermal method assured their photocatalytic activity in the visible light.[97]

Etching the DW TNT layers even longer leads to powders of individual TiO_2 nanotubes (single nanotubes, ST), also depicted in Figure 2.[95,98] ST powders revealed an excellent photocatalytic performance in the liquid phase due to the largest available area in comparison with DW and SW TNT layers[95] and thus the number of active sites. However, the small size of STs complicate the separation of ST powders from the liquid phase after the photocatalytic degradation. Therefore, a decoration of the ST powders with Fe_3O_4 was suggested, resulting in magnetically guidable ST powders, which can be advantageously used as movable photocatalysts. Furthermore, due to the bandgap of Fe_3O_4, a photocatalytic activity of such photocatalysts in the visible light was revealed.[95] A recent follow-up study[98] on this work studied the crystallinity of ST powders, showing that the combined effects of annealing, the size of crystallites, and the specific surface area enhance the photocatalytic activity of these materials. This study also revealed the interesting fact that upon annealing of the ST powders up to 800°C pure anatase phase is formed, which is unique among TiO_2 nanostructures.[98] Only upon annealing at 900°C x-ray diffraction measurements showed the formation of rutile phase, confirming that ST powders crystallize completely differently than TNT layers attached to Ti substrates, where rutile phase is usually found upon annealing at ~500°C.[99,100]

1.3 | Bipolar electrochemistry for TNT layer preparation

Most frequently, TNT layers are produced in a two-electrode set-up, using the Ti substrate as anode. The cathode can be made of any suitable material, for example, Pt, graphite, or a second Ti substrate. The easiest possibility to build the electrochemical cell is to take a beaker with the electrolyte and immerse anode and cathode into it, connected to the potentiostat. Such a typical two-electrode set-up (further denoted as "conventional") is shown in Figure 3A. It can be used to grow TNT layers over the whole area of the Ti anode immersed into the electrolyte. A more advanced conventional set-up is the use of home-designed electrochemical cells, with the Ti anode in form of a Ti foil or sheet being pressed against an O-ring from outside the cell, leaving an area of pre-defined size in contact with the electrolyte. These cells are usually employed, when only a certain area of the Ti substrate or just one side of it should be anodized. In such conventional set-ups, TNT layers with homogenous thickness and diameter are produced over the complete area of the Ti substrate being in contact with the electrolyte. On the other hand, it is not possible to produce TNT layers with a gradient in nanotube diameter and thickness in a conventional set-up. Furthermore, it is limited to Ti substrates that (i) can be connected

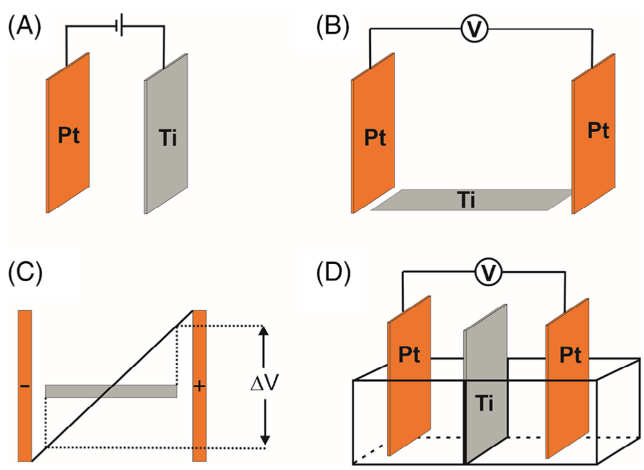

FIGURE 3 Scheme of (A) a conventional anodization set-up, (B) an open bipolar set-up, (C) potential distribution in an open bipolar set-up, and (D) a closed bipolar set-up.

to the potentiostat, and (ii) do not need to be anodized over the complete surface as a connection to the potentiostat must be established.

However, the preparation of TNT layers with a gradient in layer thickness and nanotube diameter can be of interest, for instance for a fast screening of optimal nanotube dimensions for specific applications without the need of producing several TNT layers with different dimensions to be tested for applications one by one, resulting in a time consuming and expensive procedure. To overcome this issue, bipolar electrochemistry[101–103] can be used, which is until now the only method that offers the possibility of producing gradient TNT layers. A scheme of an open electrochemical cell for the anodization of Ti substrates using bipolar electrochemistry (further denoted as "open bipolar cell") is shown in Figure 3B. In a bipolar cell, the Ti substrate is polarized in the electrical field between two so-called feeder electrodes, which are connected to the potentiostat. The Ti substrate itself is not connected to the potentiostat but fixed in the middle between the feeder electrodes, with the positively polarized side facing the feeder cathode and the negatively polarized side facing the feeder anode. The feeder electrodes should be made of an inert material, for instance Pt, to avoid side reactions. If the potential between the feeder electrodes is high enough, reactions can be driven on the Ti substrate, meaning, if a proper electrolyte is employed, it will be anodized towards TNT layer formation. The polarization potential, which arises at the Ti substrate, changes along the Ti substrate, with the highest polarization being on its extremities, while it gradual decreases towards the middle of the Ti substrate—see Figure 3C.[103] However, the anodization potential influences the nanotube diameter and growth rate.[19] Thus, when using an open bipolar cell, the TNT layers prepared will have a gradient in TNT layer thickness and nanotube diameter. The thickest nanotubes with the largest diameter grow on the edges or extremities of the Ti substrate, while thinner nanotubes with smaller diameter can be found towards its middle.[104] Simultaneously, hydrogen evolution occurs on the positively polarized extremity of the Ti substrate, as well as on the feeder cathode, due to reduction of the electrolyte. On the feeder anode oxygen is produced stemming from the oxidation of water, assuming inert feeder electrodes are employed.[105]

Although the concept of bipolar electrochemistry is known for several decades,[101,106] the use of an open bipolar cell for anodization of Ti substrates towards TNT layers was shown for the first time only in 2014 by Loget et al.[104] In this proof-of-concept study it was shown that the gradient in nanotube dimensions can be influenced by the potential applied between the feeder electrodes and the anodization time. Furthermore, the TNT layers with gradients in dimensions were employed for a fast screening of optimal TNT layer dimensions for photocurrent measurements and, after sensitization with a ruthenium-based dye, for dye sensitized solar cells (DSSCs).[104] Since then, several publications reported on the optimization of gradient TNT layer preparation, by evaluating the influence of the potential applied between the feeder electrodes,[107] by anodizing several Ti substrates simultaneously,[108] or by superimposing the TNT layer formation on a conventional electrode set-up with a bipolar set-up, resulting in a linear gradient of nanotube layer thickness and diameter along the Ti substrate.[109] A study calculating the polarization potential on different places along the Ti substrate was recently published by Zhang et al.[105] As mentioned above, the gradient TNT layers have been used for high-throughput screening of the optimal nanotube dimensions for their use in different applications; in DSSCs,[104] H_2 evolution on Pt-loaded TNT layers,[110] Li-ion batteries[107] and cell proliferation and adhesion for the possible implant modification with TNT layers.[111,112] Additionally, it was shown that gradient TNT layers perform better in Li-ion batteries at high C-rates, compared to homogeneous TNT layers.[107]

As the development of the 3D printing technology proceeds, the preparation of more complicated and individual Ti substrates also becomes more feasible. Meanwhile metallic 3D Ti and Ti alloy substrates can be printed.[113–121] A photograph of such Ti substrates is shown in Figure 4A. This is especially of interest, as in the recent years a trend was seen towards the anodization of Ti substrates with higher surface area, such as planar meshes,[122,123] as they show a superior photocatalytic performance than planar, solid Ti substrates, such as foils, due to their increased surface area and the possibility of employing them in flow-through reactors. As the anodization in a bipolar cell is wireless, meaning no connection between the Ti substrate and the potentiostat needs to be established, it is definitively very suitable for the TNT layer preparation on Ti substrates which cannot be directly connected to the potentiostat, as for instance small Ti spheres or more complicated 3D printed Ti substrates.[124–126] Inspired by the earlier work from Asoh et al. on porous Al_2O_3 layer preparation,[127–129] TNT layers were be prepared over the whole surface of such more complicated substrates by applying an alternating instead of a direct potential.[124–126] Using an alternating potential, the polarization of the Ti substrate changes its direction by a given frequency, alternating the side of the Ti substrate which is positively polarized and therefore anodized. Meanwhile, a reduction reaction happens on the negatively polarized side, meaning H_2 evolution, and, if the side was anodized previously, the prepared TNT layer will be reduced.[124] Depending on the potential applied between the feeder electrodes and

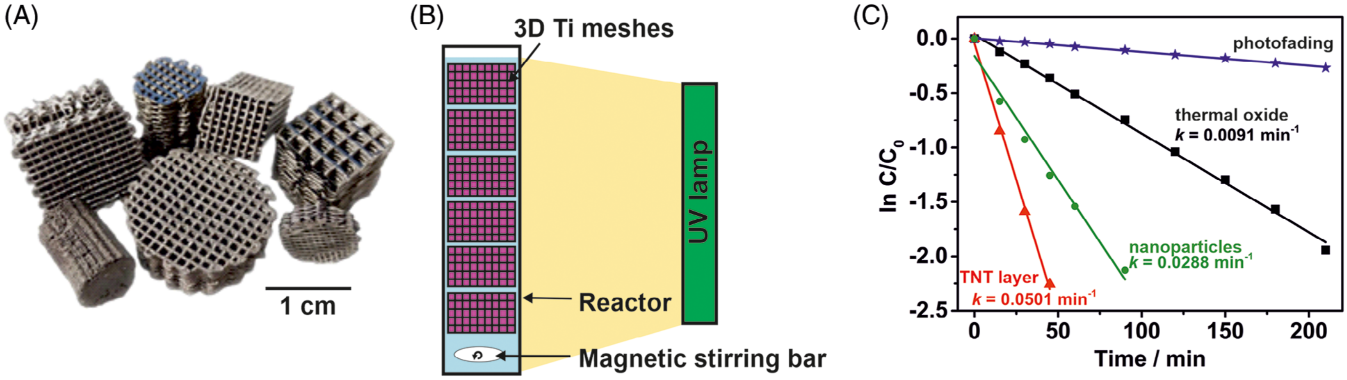

FIGURE 4 (A) Photograph of 3D printed Ti meshes, (B) photoreactor for photocatalysis in the liquid phase, (C) photocatalytic degradation kinetic curves of methylene blue using 3D printed Ti meshes with different surface modifications.

the distance of the feeder electrodes to the Ti substrate, TNT layers with different thickness and nanotube diameter can be obtained. However, one must note that rationally also under the application of an alternating potential, TNT layers with gradients in thickness and diameter are produced. In this case, if the anodization was carried out with an alternating potential of equal amplitude and an equal distance of the Ti substrate to both feeder electrodes, TNT layers with a homogenous gradient from the Ti substrate´s extremities to its middle are produced.[124]

The application of Ti spheres[124] and 3D Ti and Ti alloy meshes[125,126] modified with TNT layers by bipolar electrochemistry under alternating potentials has been shown for photocatalysis in the liquid[124,125] as well as in the gas phase.[126] A scheme of a photocatalytic reactor for pollutant degradation in the liquid phase, using anodized Ti meshes as photocatalyst, is shown in Figure 4B.[125] Compared to their counterparts modified with thin thermal TiO_2 layers or TiO_2 nanoparticles, the TNT layer modified Ti meshes revealed significantly increased photocatalytic degradation rates, due to the highly increased surface area – see Figure 4C.[124,125]

Instead of using the above-described open bipolar set-up, also a closed bipolar set-up can be employed for the anodization of Ti substrates. The scheme of a closed bipolar set-up is shown in Figure 3D. The set-up consists of two half cells with the Ti substrate as separator. Each half cell contains one feeder electrode. Compared to the open bipolar set-up, the closed set-up has the advantage that the potential at the Ti substrate is the same as the potential applied at the feeder electrodes, as the entire current must flow through the Ti substrate. This results in the possibility of applying much lower potentials between the feeder electrodes, than in an open bipolar set-up.[130,131] Additionally, the polarization of the Ti substrate occurs homogeneously without any gradient in the potential, resulting in Ti layers with homogeneous thickness and diameter on the Ti substrate´s surface.[132,133]

An easy way to build a closed bipolar set-up for the anodization of Ti, as well as of Al was shown by Chen et al.[133] and Xu et al.,[134] respectively, who used two beakers as half cells and the Ti or Al substrate, respectively, as bridge between the beakers. A more elegant set-up was used by Sopha et al.,[132] who designed a two-compartment cell allowing the Ti substrate to be fixed between two O-rings in its middle. Naturally, applying a direct potential to a closed bipolar set-up leads to TNT layers on one side of the Ti substrate, while applying an alternating potential to TNT layers on both sides. The TNT layer dimensions are the same as for TNT layers prepared in a conventional set-up under the same anodization conditions.[132]

However, the closed bipolar set-up becomes an exciting choice for the modification of Ti substrates with different dimensions on both sides. This can be done by using alternating potentials of different amplitude in both half-cells or even by using completely different electrolytes in both half-cells.[132] This can be interesting for applications, in which different TNT layers on one Ti substrate are needed. In comparison, in a conventional set-up, one side of the Ti substrate must be protected from contact with the electrolyte during anodization and both sides must be anodized after each other to receive the Ti substrates with TNT layers of different dimensions on both sides, making it tremendously more tedious.

1.4 | Application of TNT layers in microwave sensors

Although microwave resonator sensors are known for a long time,[135] the use of TNT layers as sensing material for them is less explored. The principle of microwave resonator sensors is based on the interaction of the electromagnetic waves with the tested matter. Due to this interaction, changes in the permittivity of the material can be detected, which manifest as a frequency change or amplitude attenuation of the microwave signal.[136]

Microwave resonator sensors are employed in different applications (e.g., medicine or environmental monitoring),[137] as they can be used for real-time monitoring, reveal a high resolution and can accurately identify various solids, liquids and gases. One possible application is the detection of ultraviolet (UV) light, which has captured considerable significant interest,[138–140] due to the potential health risks by excessive UV irradiation, leading for instance to premature skin aging and skin cancer.[141] UV sensors are frequently needed in different sectors of industry.[142–144] For this, planar microwave resonator sensors have demonstrated a compelling performance, due to a high sensitivity, inexpensiveness, and robustness. Furthermore, they possess a high signal-to-noise ratio (quality factor), real-time responsiveness, and a simple operation in an electrode-less design. It is possible to miniaturize these sensors, and they are compatible with the complementary metal-oxide-semiconductor (CMOS) technology.[136,145,146]

In a pioneering proof-of concept study, Zarifi et al.[145] demonstrated for the first time the possibility of integrating freestanding TNT layers, obtained by delaminating the TNT layers from the underlying Ti substrates, into planar microwave resonator sensors for the aim of UV light sensing. A persistence of charged pair states within the freestanding TNT layers for several hours was observed, as well as a dependency of changes in the dielectric properties (as permittivity and electrical conductivity) on both the UV light´s wavelength and intensity of the incident light.[145] The changes of the dielectric properties lead to an observable shift in the sensor response, either in the resonant amplitude or in the resonant frequency. A typical experimental set-up for such freestanding TNT layer integrated planar microwave resonator sensors is shown in Figure 5A.

Subsequently, follow-up studies were focused on increasing the sensitivity and lowering the detection limits of the freestanding TNT layer integrated microwave resonator sensors towards the UV light.[146–148] This was carried out either by optimizing the sensor design and operation parameters (i.e., operating frequency and amplitude)[147,148] or by decorating the freestanding TNT layers with Au nanoparticles.[146] It was found that the use of a high-frequency resonator offers several advantages, including the ability to mitigate noise caused by water vapor and environmental contaminants, making it a promising candidate for sensitive and accurate UV detection.[148] In case of Au nanoparticle decorated freestanding TNT layers, a significantly increased temporal microwave response was recorded upon UV light irradiation compared to blank freestanding TNT layers, which was attributed to the a faster and more persistent charge separation at the Au/TiO_2 heterojunction.[146] Additionally, it was shown that such freestanding TNT layer integrated microwave resonator sensors can be employed also in the liquid phase for UV light detection.[136]

While in these mentioned pioneering studies[136,145–148] the sensor design and the operation parameters have been optimized, the influence of the freestanding TNT layer thickness and the aspect ratio of the TNTs has not been investigated. The thickness of the employed freestanding TNT layers was mainly ranging between 13 and 20 μm, revealing relatively low aspect ratio. Only one study employed HAR freestanding TNT layers (thickness 115 μm, AR 920), with the aim to distinguish between deep trapping transients of electrons and holes in the freestanding TNT layers.[149] However, no optimization of the freestanding TNT layer thickness or its AR was carried out.

Therefore, a recent study by Alijani et al.[150] investigated the impact of HAR freestanding TNT layers on the microwave-photoresponse using planar microwave resonator sensors to optimize the sensor performance. Freestanding TNT layers with different thicknesses (i.e., 15, 50, 80, and 110 μm; AR between 60 and 733) were employed. The results revealed that the microwave response was notably influenced by the layer thickness, with the 80 μm thick freestanding TNT layers being the most responsive ones to UV light – see Figure 5B. The differences were attributed to trapped electrons interacting with electromagnetic waves. A scheme illustrating the patterns of UV adsorption and the penetration of microwave signals for freestanding TNT layers with different thickness is shown in Figure 5C. This work enhanced the understanding of the thickness-dependent microwave photoconductivity in TNT layers, leading to an improvement of the UV sensing device.[150]

In another study,[151] the optimal 80 μm thick freestanding TNT layers were integrated into a passive split-ring resonator (SRR) tag, which was coupled with an active feedback-assisted SRR reader, enabling high-resolution UV detection. It was found that by combining the passive tag with active SRR reader losses were mitigated and the sensitivity of the sensors was significantly improved, leading to very accurate UV detection. This study offers a robust solution for high-resolution UV detection in diverse industrial and biomedical applications.

The results showed that the freestanding TNT layer-integrated microwave resonator sensors are a promising option for UV sensing applications. Their high sensitivity, accuracy, repeatability, and ability to operate at high frequencies make them suitable for diverse fields such as medical, environmental, and process monitoring.

Light detection is not just relevant in the UV but also in the visible light spectrum, as it may be used in quality or purity analyses for health and safety applications.[152] However, due to the wide bandgap of TiO_2 of 3.2 eV,

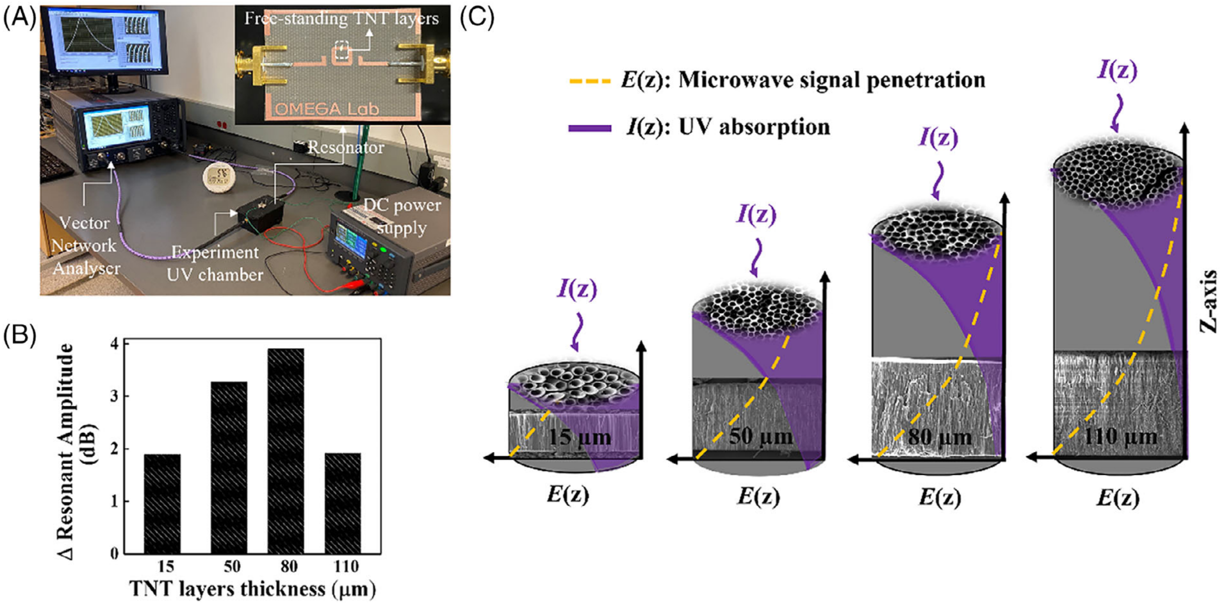

FIGURE 5 A, Instrumentation and experimental setup of a microwave resonator sensor. The inset shows the positioning of free-standing TNT layers within the ring gap of the resonator; (B) Measurement of resonant amplitude shift for different freestanding TNT layer thicknesses (15, 50, 80, 110 μm); (C) Scheme of the patterns of UV absorption (purple) and penetration of microwave signals (yellow dashed line), illustrating their interaction zones for different freestanding TNT layer thicknesses (15, 50, 80, 110 μm). TNT, TiO_2 nanotube.

the freestanding TNT layers themselves cannot be used as sensing layer for visible light detection. To overcome this challenge, freestanding TNT layers with a 5 nm thin coating of CdS prepared by ALD were employed as sensing layer in planar microwave resonator sensors.[153] This setup yielded in a high sensitivity to green and red light, while also enhancing response rates and reducing recovery durations after the light exposure. The study suggested promising future directions, including refining the functional coating and nanotube geometry to further enhance the sensor's performance.

Although the freestanding TNT layers integrated microwave sensors were mainly used for the detection of light, it was also shown by Zarifi et al.[154] that such sensors can be used for the detection of analytes in the liquid phase. This study demonstrated that in aqueous solutions KOH concentration as low as 0.1 mM can be detected.

1.5 | Upscaling of the nanotube layers – Towards real-life applications

Though the applications of TNT layers are widely exploited and discussed in the literature, surprisingly small efforts were spent in the last 20 years to produce them on Ti substrates larger than a few cm^2. While TNT layers on small areas may be sufficient for some applications, such as for instance sensing devices, TNT layers produced on much larger area substrates are required for other applications, as for photocatalytic devices or solar cells. However, though the initial tests and optimization of the TNT layers´properties may be carried out on the laboratory scale, for an application in industrial produced devices used in real-life it must be possible to produce TNT layers on Ti substrates of larger area than a few cm^2.

Especially for their use in the photocatalytic degradation of pollutants in the liquid as well as in the gaseous phase, TNT layers showed superior results compared to their nanoparticulate counterparts, which are frequently used (see Figure 6).[155,156] Therefore, within the last years, several reports on upscaling of TNT layer size were

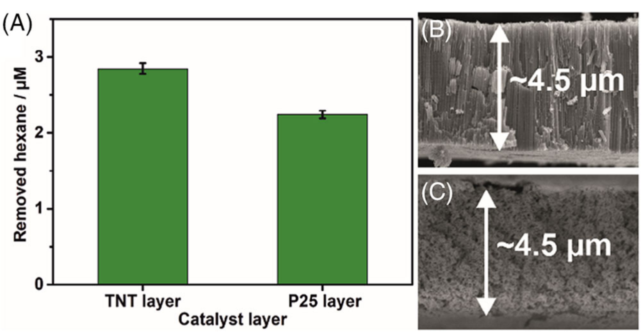

FIGURE 6 A, Photocatalytic hexane removal in the gas phase using either a TNT layer or a nanoparticle layer of P25 as photocatalyst, and the corresponding cross-sectional SEM images of the (B) TNT and (C) nanoparticle layers. TNT, TiO_2 nanotube.

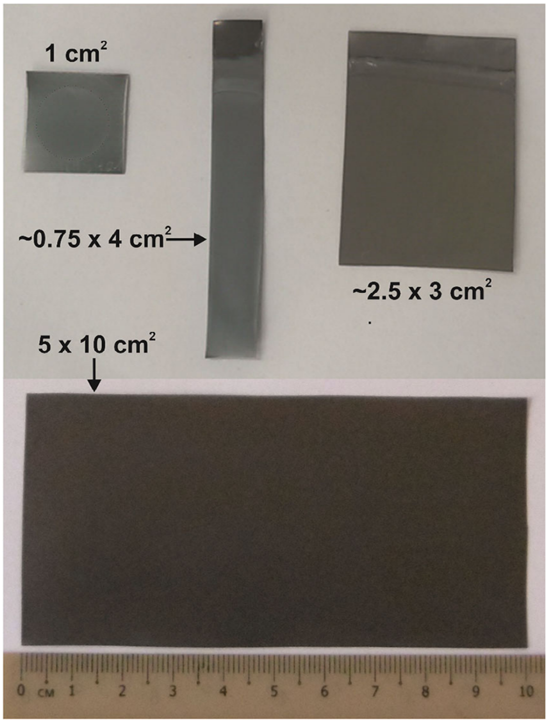

FIGURE 7 Illustrative photographs of TNT layers of different size, demonstrating the development of Ti substrate sizes over the years. The dimensions of nanotube layers on individual samples are not necessarily the same. TNT, TiO_2 nanotube.

published, mainly for their possible use in photocatalytic applications.[122,125,126,156–166] Illustrative photographs of TNT layers prepared on Ti substrates from 1 to 50 cm^2 are shown in Figure 7, showing the upscaling of the Ti substrate size within the years. However, increasing the Ti substrate´s surface for TNT layer production turned out to be more difficult than expected. The main problem is the high absolute current flowing between the two electrodes which increases with the area to be anodized, leading to Joule heating and an increase in electrolyte temperature. This enhances the likelihood of the occurrence of dielectric breakdown,[71,72] hampering the TNT layer synthesis, as explained before in chapter 1.1.[75]

To overcome this problem, different approaches have been applied. One of the most obvious approaches is stirring of the electrolyte during anodization, resulting in a transport of the heat generated at the anode (at the growing TNT layer) into the entire electrolyte volume. This stirring could for instance be carried out by magnetic or mechanical stirring, although this easiest of all approaches has not been published for the anodization of large substrates. Mena et al.[165] however stirred the electrolyte by a continuous circulation from a reservoir through the electrochemical cell by employing a pump. The design of electrolyte circulation by a pump additionally has the advantage of a possible continuous supply of fresh electrolyte, if required.[165] Additionally, in such an anodization set-up the electrolyte in the reservoir has the possibility to cool down, while not being used or even might be actively cooled externally. However, stirring of the electrolyte also increases the current density recorded compared to anodization in a non-stirred electrolyte,[167–169] as the movement of ions is not solely due to diffusion and might therefore be counterproductive.

Another approach is to use electrolytes, which require rather low anodization potentials, such as aqueous electrolytes or electrolytes with a high water content.[158,161,166] In such electrolyte usually a low potential is applied and due to the high etching rates the anodization times are comparably short, as described in Chapter 1.2. Alternatively, comparably low anodization potentials for a relatively short time can be applied for highly viscous electrolytes, which usually used with high anodization potentials and long anodization times to receive relatively thick TNT layers.[122,157,160,162–165] As a result, the current flowing between the electrodes is comparably low and/or just flowing for a short time, which results in a low temperature increase of the electrolyte and therefore reduced possibility of dielectric breakdown. On the other hand, under these conditions, the received TNT layers are relatively thin, between approximately 500 nm and a few µm (AR between ~6 and ~65).[122,157,158,161,163–166] Additionally to a low anodization potential and short anodization time in a viscous ethylene glycol-based electrolyte, Lincho et al.[157] also used an extremely high electrolyte volume of 8 L to disperse the Joule heat generated during the anodization of a 600 cm^2 large Ti substrate.

However, experiments on the laboratory scale have shown that for instance for the photocatalytic degradation of pollutants, thicker TNT layers show superior degradation rates compared to thinner layers.[155,170,171] Therefore, also on the large scale thicker TNT layers must be prepared with the motivation to improve their photocatalytic performance. Recently, the preparation of TNT layers of different thicknesses up to 14 µm (AR up to ~107) on 100 cm^2 large Ti substrates was shown.[159] In this publication, the electrolytes were significantly cooled during anodization to countervail the temperature increase due to the Joule heating and additionally the electrolyte age was carefully optimized for electrolytes with different composition individually.[159] The key is that the electrolyte composition changes with every time it was used for anodization (see also Chapter 1.1), resulting in lower current densities recorded during anodization.[75,77] Therefore, in older electrolytes higher potentials can be applied with a lower possibility of dielectric breakdown. These higher anodization potentials lead to a faster growth rate and therefore to thicker TNT layers. However, laboratory conditions also play a significant role in the aging of an electrolyte. For instance, if the electrolyte is hygroscopic, the water content increases with time when it is in contact with air, resulting in an overall change of its composition. This is especially the case for ethylene-based electrolytes and could only be completely circumvented by working in air-tight conditions (e.g., in a glove box). Thus, a balance must be found for the preparation of thick TNT layers on the large scale between electrolyte age and composition, and the anodization potential for each electrolyte individually, taking the laboratory conditions into account.[159] Nonetheless, the mentioned study shows that this is possible.[159]

Overall, the recent studies show, that the TNT layers on the large scale (considered as opposite to small, a few cm^2 sized TNT layers on the laboratory scale) have the potential to be employed in real-life applications, particularly for the photocatalytic degradation of pollutants. Under ISO standards applied for photocatalytic degradation of pollutants in the gas phase, TNT layers outperformed P25 nanoparticle layers[156] and the by now thickest prepared and applied TNT layers of 14 μm thickness on large Ti substrates clearly revealed the highest degradation rates.[159] This shows that still some research is needed to optimize the TNT layer preparation on large areas and increase their thickness for optimal performance in real-life applications. However, a first step was made, paving the way.

2 | CONCLUSION

In this mini review, an overview of the recent developments in the TNT layer research was given. It seems to be clear that many aspects of the TNT layer synthesis and their general applications are deeply investigated meanwhile. Nonetheless, new application possibilities, as the use of TNT layers in microwave sensors, are still to be exploited in more detail. Meanwhile, the synthesis by means of bipolar electrochemistry opens the doors towards the growth of TNT layers on more complex, such as 3D printed, Ti substrates and their possible use in new applications.

Additionally, it must be pointed out that the application of TNT layers and their ST powders in the photocatalytic degradation of pollutants, in the liquid as well as in the gas phase, is meanwhile very well studied, frequently showing a superior performance of TNT layers compared to nanoparticulate layers, which are the most frequently used TiO_2 based photocatalysts. It is therefore of high interest that the possibilities of upscaling the TNT layers from the laboratory scale to the full scale for real-life applications are properly investigated. Though the cited initial studies may pave the way towards the full scale, deeper investigations and more research efforts are still necessary.

ACKNOWLEDGMENTS

The authors acknowledge the Ministry of Education, Youth and Sports of the Czech Republic (MEYS CR, project LM2023037). The authors also thank the COST action (CA20126, "NETPORE") for the support.

DATA AVAILABILITY STATEMENT

The data that support the findings of this study are available from the corresponding author upon reasonable request.

1. A. Fujishima, K. Honda, *Nature* **1972**, *238*, 37.
2. M. R. Hoffmann, S. T. Martin, W. Choi, D. W. Bahnemann, *Chem. Rev.* **1995**, *95*, 69.
3. B. O´Regan, M. Grätzel, *Nature* **1991**, *353*, 737.
4. U. Kirner, K. D. Schierbaum, W. Göpel, B. Leibold, N. Nicoloso, W. Weppner, D. Fischer, W. F. Chu, *Sensors Actuators* **1990**, *B1*, 103.
5. Y.-T. Sul, C. B. Johansson, S. Petronis, A. Krozer, Y. Jeong, A. Wennerberg, T. Albrektsson, *Biomaterials* **2002**, *23*, 491.
6. U. Diebold, *Surf. Sci. Rep.* **2003**, *48*, 53.
7. A. L. Linsebigler, G. Lu, J. T. Yates, *Chem. Rev.* **1995**, *95*, 735.
8. X. Chen, C. Li, M. Grätzel, R. Kostecki, S. S. Mao, *Chem. Soc. Rev.* **2012**, *41*, 7909.
9. E. Scolan, C. Sanchez, *Chem. Mater.* **1998**, *10*, 3217.
10. M. Lafjah, A. Mayoufi, E. Schaal, F. Djafri, A. Bengueddach, N. Keller, V. Keller, *Catal. Today* **2014**, *235*, 193.
11. S. Yoo, S. A. Akbar, K. H. Sandhage, *Adv. Mater.* **2004**, *16*, 260.
12. M. Assefpour-Dezfuly, C. Vlachos, E. H. Andrews, *J. Mater. Sci.* **1984**, *19*, 3626.
13. V. Zwilling, M. Aucouturier, E. Darque-Ceretti, *Electrochim. Acta* **1999**, *45*, 921.
14. T. Kasuga, M. Hiramatsu, A. Hoson, T. Sekino, K. Niihara, *Langmuir* **1998**, *14*, 3160.
15. P. Hoyer, *Langmuir* **1996**, *12*, 1411.
16. D. Li, Y. Xia, *Nano Lett.* **2003**, *3*, 555.
17. J. M. Macak, P. Schmuki, *Electrochim. Acta* **2006**, *52*, 1258.
18. V. Thavasi, V. Renugopalakrishnan, R. Jose, S. Ramakrishna, *Mater. Sci. Eng. R Reports* **2009**, *63*, 81.
19. J. M. Macak, H. Tsuchiya, A. Ghicov, K. Yasuda, R. Hahn, S. Bauer, P. Schmuki, *Curr. Opin. Solid State Mater. Sci.* **2007**, *11*, 3.
20. K. Lee, A. Mazare, P. Schmuki, *Chem. Rev.* **2014**, *114*, 9385.
21. A. G. Reynaud Morales, M. O. Concha Guzmán, C. Cuevas Arteaga, *Corros. Rev.* **2011**, *29*, 105.
22. F. Riboni, N. T. Nguyen, S. So, P. Schmuki, *Nanoscale Horiz.* **2016**, *1*, 445.
23. H. Sopha, J. M. Macak, In *Nanostructured Anodic Met. Oxides*, G. D. Sulka, Ed. Elsevier Inc., Amsterdam, **2020**, pp. 173–209.
24. X. Zhou, N. T. Nguyen, S. Özkan, P. Schmuki, *Electrochem. commun.* **2014**, *46*, 157.
25. A. Ghicov, P. Schmuki, *Chem. Commun.* **2009**, 2791. https://doi.org/10.1039/B822726H
26. D. Regonini, C. R. Bowen, A. Jaroenworaluck, R. Stevens, *Mater. Sci. Eng. R Reports* **2013**, *74*, 377.
27. D. Kowalski, D. Kim, P. Schmuki, *Nano Today* **2013**, *8*, 235.
28. P. Roy, S. Berger, P. Schmuki, *Angew. Chemie Int. Ed.* **2011**, *50*, 2904.

29. F. Dvorak, R. Zazpe, M. Krbal, H. Sopha, J. Prikryl, S. Ng, L. Hromadko, F. Bures, J. M. Macak, *Appl. Mater. Today* **2019**, *14*, 1.
30. I. Paramasivam, H. Jha, N. Liu, P. Schmuki, *Small* **2012**, *8*, 3073.
31. S. Palmas, L. Mais, M. Mascia, A. Vacca, *Curr. Opin. Electrochem.* **2021**, *28*, 100699.
32. A. Auer, J. Kunze-Liebhäuser, *Small Methods* **2019**, *3*, 1800385.
33. V. Galstyan, J. M. Macak, T. Djenizian, *Appl. Mater. Today* **2022**, *29*, 101613.
34. M.-M. Zhang, J.-Y. Chen, H. Li, C.-R. Wang, *Rare Met*. **2021**, *40*, 249.
35. P. Roy, D. Kim, K. Lee, E. Spiecker, P. Schmuki, *Nanoscale* **2010**, *2*, 45.
36. Y. Xu, G. Zangari, *Coatings* **2021**, *11*, 931.
37. S. Minagar, J. Wang, C. C. Berndt, E. P. Ivanova, C. Wen, *J. Biomed. Mater. Res. Part A* **2013**, *101A*, 2726.
38. M. Kulkarni, A. Mazare, E. Gongadze, Š. Perutkova, V. Kralj-Iglič, I. Milošev, P. Schmuki, A Iglič, M. Mozetič, *Nanotechnology* **2015**, *26*, 062002.
39. Y. Fu, A. Mo, *Nanoscale Res. Lett.* **2018**, *13*, 187.
40. J. Park, A. Cimpean, A. B. Tesler, A. Mazare, *Nanomaterials* **2021**, *11*, 2359.
41. C. C. Raj, R. Prasanth, *J. Electrochem. Soc.* **2018**, *165*, E345.
42. V. Galstyan, E. Comini, G. Faglia, G. Sberveglieri, *Sensors* **2013**, *13*, 14813.
43. K. Inoue, A. Matsuda, G. Kawamura, *Sci. Rep.* **2023**, *13*, 103.
44. M. M. Abouelela, K. Inoue, G. Kawamura, W. K. Tan, A. Matsuda, *Sustain. Mater. Technol.* **2023**, *38*, e00718.
45. S. McMichael, A. Tolosana-Moranchel, M. A. L. R. M. Cortes, J. W. J. Hamilton, P. Fernandez-Ibanez, J. A. Byrne, *Appl. Catal. B Environ.* **2022**, *311*, 121339.
46. C. Adán, C. Pablos, P. Misis, S. Pascua, J. Marugán, *Sci. Total Environ.* **2023**, *894*, 165017.
47. H. Sopha, C. Ghigo, S. Ng, M. Alijani, L. Hromadko, J. Michalicka, T. Djenizian, J. M. Macak, *Mater. Chem. Phys.* **2022**, *276*, 125337.
48. S. Dasarathan, M. Ali, T. J. Jung, J. Sung, Y. C. Ha, J. W. Park, D. Kim, *Nanomaterials* **2021**, *11*, 1.
49. M. Vincent, D. Kowalski, *ACS Appl. Nano Mater*. **2023**, *6*, 6528.
50. S. Dasarathan, J. Sung, J.-W. Hong, Y.-S. Jo, B. G. Kim, Y.-J. Lee, H.-Y. Choi, J.-W. Park, D. Kim, *RSC Adv*. **2023**, *13*, 8299.
51. S. Yahya Rahnamaee, R. Bagheri, M. Vossoughi, M. khafaji, E. Asadian, S. Ahmadi Seyedkhani, A. Samadikuchaksaraei, *Appl. Surf. Sci.* **2022**, *580*, 152263.
52. K. Staats, M. Pilz, J. Sun, T. Boiadjieva-Scherzer, H. Kronberger, S. Tobudic, R. Windhager, J. Holinka, *Sci. Rep.* **2022**, *12*, 8298.
53. I. C. Turu, S. Bayraktar, B. Akgul, E. Ilhan-Sungur, E. S. Abamor, N. Cansever, *Surf. Coatings Technol.* **2023**, *470*, 129866.
54. K. Baishya, K. Vrchovecká, M. Alijani, J. Rodriguez-Pereira, S. M. Thalluri, M. P. Goldbergová, J. Přibyl, J. M. Macak, *Appl. Surf. Sci. Adv.* **2023**, *18*, 100459.
55. N. Taghvaei, E. Taghvaei, M. Askari, *ChemistrySelect* **2020**, *5*, 10339.
56. R. Beranek, H. Hildebrand, P. Schmuki, *Electrochem. Solid-State Lett.* **2003**, *6*, B12.
57. D. Gong, C. A. Grimes, O. K. Varghese, W. Hu, R. S. Singh, Z. Chen, E. C. Dickey, *J. Mater. Res.* **2001**, *16*, 3331.
58. J. M. Macák, H. Tsuchiya, P. Schmuki, *Angew. Chemie Int. Ed.* **2005**, *44*, 2100.
59. J. M. Macak, K. Sirotna, P. Schmuki, *Electrochim. Acta* **2005**, *50*, 3679.
60. A. Ghicov, H. Tsuchiya, J. M. Macak, P. Schmuki, *Electrochem. commun.* **2005**, *7*, 505.
61. J. M. Macak, H. Tsuchiya, L. Taveira, S. Aldabergerova, P. Schmuki, *Angew. Chemie Int. Ed.* **2005**, *44*, 7463.
62. S. P. Albu, A. Ghicov, J. M. Macak, P. Schmuki, *Phys. status solidi – Rapid Res. Lett.* **2007**, *1*, R65.
63. M. Paulose, H. E. Prakasam, O. K. Varghese, L. Peng, K. C. Popat, G. K. Mor, T. A. Desai, C. A. Grimes, *J. Phys. Chem. C* **2007**, *111*, 14992.
64. K. Shankar, G. K. Mor, H. E. Prakasam, S. Yoriya, M. Paulose, O. K. Varghese, C. A. Grimes, *Nanotechnology* **2007**, *18*, 065707.
65. S. So, K. Lee, P. Schmuki, *J. Am. Chem. Soc.* **2012**, *134*, 11316.
66. S. So, K. Lee, P. Schmuki, *Chem.—A Eur. J.* **2013**, *19*, 2966.
67. R. Zazpe, H. Sopha, J. Prikryl, M. Krbal, J. Mistrik, F. Dvorak, L. Hromadko, J. M. Macak, *Nanoscale* **2018**, *10*, 16601.
68. S. P. Albu, A. Ghicov, J. M. Macak, R. Hahn, P. Schmuki, *Nano Lett*. **2007**, *7*, 1286.
69. H. E. Prakasam, K. Shankar, M. Paulose, O. K. Varghese, C. A. Grimes, *J. Phys. Chem. C* **2007**, *111*, 7235.
70. J.-F. Vanhumbeeck„ J. Proost, *Corros. Rev.* **2009**, *27*, 117.
71. J. M. Albella, I. Montero, J. M. Martinez-Duart, *Electrochim. Acta* **1987**, *32*, 255.
72. F. Di Quarto, S. Piazza, C. Sunseri, *J. Electroanal. Chem. Interfacial Electrochem.* **1988**, *248*, 99.
73. S. Sreekantan, L. C. Wei, Z. Lockman, *J. Electrochem. Soc.* **2011**, *158*, C397.
74. S. Banerjee, M. Misra, S. K. Mohapatra, C. Howard, S. K. Mohapatra, S. K. Kamilla, *Nanotechnology* **2010**, *21*, 145201.
75. M. Alijani, H. Sopha, S. Ng, J. M. Macak, *Electrochim. Acta* **2021**, *376*, 138080.
76. M. Alijani, H. Sopha, S. Ng, J. Rodriguez-Pereira, J. M. Macak, *Phys. status solidi – Rapid Res. Lett.* **2021**, *15*, 2100146.
77. H. Sopha, L. Hromadko, K. Nechvilova, J. M. Macak, *J. Electroanal. Chem.* **2015**, *759*, 122.
78. S. Bauer, S. Kleber, P. Schmuki, *Electrochem. commun.* **2006**, *8*, 1321.
79. S. P. Albu, A. Ghicov, S. Aldabergenova, P. Drechsel, D. LeClere, G. E. Thompson, J. M. Macak, P. Schmuki, *Adv. Mater.* **2008**, *20*, 4135.
80. C. Xue, T. Narushima, Y. Ishida, T. Tokunaga, T. Yonezawa, *ACS Appl. Mater. Interfaces* **2014**, *6*, 19924.
81. N. Liu, H. Mirabolghasemi, K. Lee, S. P. Albu, A. Tighineanu, M. Altomare, P. Schmuki, *Faraday Discuss*. **2013**, *164*, 107.
82. S. Berger, S. P. Albu, F. Schmidt-Stein, H. Hildebrand, P. Schmuki, J. S. Hammond, D. F. Paul, S. Reichlmaier, *Surf. Sci.* **2011**, *605*, L57.
83. A. Dronov, I. Gavrilin, E. Kirilenko, D. Dronova, S. Gavrilov, *Appl. Surf. Sci.* **2018**, *434*, 148.
84. S. Mohajernia, A. Mazare, I. Hwang, S. Gaiaschi, P. Chapon, H. Hildebrand, P. Schmuki, *Appl. Surf. Sci.* **2018**, *442*, 412.
85. H. Mirabolghasemi, N. Liu, K. Lee, P. Schmuki, *Chem. Commun.* **2013**, *49*, 2067.
86. S. Yoriya, M. Paulose, O. K. Varghese, G. K. Mor, C. A. Grimes, *J. Phys. Chem. C* **2007**, *111*, 13770.
87. S. P. Albu, P. Schmuki, *Phys. status solidi—Rapid Res. Lett.* **2010**, *4*, 215.
88. S. So, I. Hwang, P. Schmuki, *Energy Environ. Sci.* **2015**, *8*, 849.
89. S. So, F. Riboni, I. Hwang, D. Paul, J. Hammond, O. Tomanec, R. Zboril, D. R. Sadoway, P. Schmuki, *Electrochim. Acta* **2017**, *231*, 721.

90. I. Hwang, S. So, M. Mokhtar, A. Alshehri, S. A. Al-Thabaiti, A. Mazare, P. Schmuki, *Chem.—A Eur. J.* **2015**, *21*, 9204.
91. N. T. Nguyen, I. Hwang, T. Kondo, T. Yanagishita, H. Masuda, P. Schmuki, *Electrochem. commun.* **2017**, *79*, 46.
92. M. Motola, H. Sopha, M. Krbal, L. Hromádko, Z. O. Zmrhalová, G. Plesch, J. M. Macak, *Electrochem. commun.* **2018**, *97*, 1.
93. M. Motola, L. Hromadko, J. Prikryl, H. Sopha, M. Krbal, J. M. Macak, *Electrochim. Acta* **2020**, *352*, 136479.
94. H. Sopha, Z. Spotz, M. Sepúlveda, M. Alijani, M. Motola, L. Hromadko, J. M. Macak, *Ceram. Int.* **2023**, *49*, 24293.
95. D. Beketova, M. Motola, H. Sopha, J. Michalicka, V. Cicmancova, F. Dvorak, L. Hromadko, B. Frumarova, M. Stoica, J. M. Macak, *ACS Appl. Nano Mater.* **2020**, *3*, 1553.
96. M. Motola, R. Zazpe, L. Hromadko, J. Prikryl, V. Cicmancova, J. Rodriguez-Pereira, H. Sopha, J. M. Macak, *Appl. Surf. Sci.* **2021**, *549*, 149306.
97. K. Villa, H. Sopha, J. Zelenka, M. Motola, L. Dekanovsky, D. C. Beketova, J. M. Macak, T. Ruml, M. Pumera, *Small* **2022**, *18*, 2106612.
98. M. Sepúlveda, I. Saldan, A. Mahnaz, V. Cicmancova, J. Michalicka, L. Hromadko, R. Bulánek, H. Sopha, J. M. Macak, *Ceram. Int.* **2023**, *49*, 6764.
99. A. Ghicov, H. Tsuchiya, J. M. Macak, P. Schmuki, *Phys. Status Solidi Appl. Mater. Sci.* **2006**, *203*, 28.
100. S. Das, R. Zazpe, J. Prikryl, P. Knotek, M. Krbal, H. Sopha, V. Podzemna, J. M. Macak, *Electrochim. Acta* **2016**, *213*, 452.
101. D. C. Eardley, D. Handley, S. P. S. Andrew, *Electrochim. Acta* **1973**, *18*, 839.
102. S. E. Fosdick, K. N. Knust, K. Scida, R. M. Crooks, *Angew. Chemie Int. Ed.* **2013**, *52*, 10438.
103. G. Loget, D. Zigah, L. Bouffier, N. Sojic, A. Kuhn, *Acc. Chem. Res.* **2013**, *46*, 2513.
104. G. Loget, S. So, R. Hahn, P. Schmuki, *J. Mater. Chem. A* **2014**, *2*, 17740.
105. Q. Zhang, H. Zhou, M. Yang, X. Tang, Q. Hong, Z. Yang, S. Liu, J. Chen, G. Zhou, C. Pan, *J. Electroanal. Chem.* **2022**, *915*, 116337.
106. F. Goodridge, C. J. H. King, A. R. Wright, *Electrochim. Acta* **1977**, *22*, 1087.
107. W. Wei, F. Björefors, L. Nyholm, *Electrochim. Acta* **2015**, *176*, 1393.
108. M. Saqib, J. Lai, J. Zhao, S. Li, G. Xu, *ChemElectroChem* **2016**, *3*, 360.
109. J. Wu, M. Li, Y. Zhou, W. Geng, X. Li, K. Li, K. Xu, Y. Yang, P. Gao, K. Cai, *Scr. Mater.* **2022**, *221*, 114947.
110. G. Loget, P. Schmuki, *Langmuir* **2014**, *30*, 15356.
111. P. Mu, Y. Li, Y. Zhang, Y. Yang, R. Hu, X. Zhao, A. Huang, R. Zhang, X. Liu, Q. Huang, C. Lin, *ACS Biomater. Sci. Eng.* **2018**, *4*, 2804.
112. Y. Li, S. Wang, Y. Dong, P. Mu, Y. Yang, X. Liu, C. Lin, Q. Huang, *Bioact. Mater.* **2020**, *5*, 1062.
113. C. Oliver-Urrutia, A. Kashimbetova, K. Slámečka, L. Čelko, E. B. Montufar, *Trans. Indian Inst. Met.* **2023**, *76*, 389.
114. E. B. Montufar, S. Tkachenko, M. Casas-Luna, P. Škarvada, K. Slámečka, S. Diaz-de-la-Torre, D. Koutný, D. Paloušek, Z. Koledova, L. Hernández-Tapia, T. Zikmund, L. Čelko, J. Kaiser, *Addit. Manuf.* **2020**, *36*, 101516.
115. P. Zhao, Y. Liu, T. Li, Y. Zhou, S. Leeflang, L. Chen, C. Wu, J. Zhou, Z. Huan, *Prog. Nat. Sci. Mater. Int.* **2020**, *30*, 502.
116. K. Gulati, M. Prideaux, M. Kogawa, L. Lima-Marques, G. J. Atkins, D. M. Findlay, D. Losic, *J. Tissue Eng. Regen. Med.* **2017**, *11*, 3313.
117. S. Maher, G. Kaur, L. Lima-Marques, A. Evdokiou, D. Losic, *ACS Appl. Mater. Interfaces* **2017**, *9*, 29562.
118. S. Bose, D. Banerjee, A. Shivaram, S. Tarafder, A. Bandyopadhyay, *Mater. Des.* **2018**, *151*, 102.
119. K. Nune, R. Misra, X. Gai, S. Li, Y. Hao, *J. Biomater. Appl.* **2018**, *32*, 1032.
120. B. Ren, Y. Wan, C. Liu, H. Wang, M. Yu, X. Zhang, Y. Huang, *Mater. Sci. Eng. C* **2021**, *118*, 111505.
121. C.-Y. Lee, A. C. Taylor, S. Beirne, G. G. Wallace, *Adv. Energy Mater.* **2017**, *7*, 1701060.
122. M. Motola, L. Satrapinsky, T. Roch, Š. Jan, J. Kupčík, M. Klementová, M. Jakubičková, F. Peterka, G. Plesch, *Catal. Today* **2017**, *287*, 59.
123. L. Qiu, Q. Wang, Z. Liu, Q. Zhao, X. Tian, H. Li, S. Gao, *Sep. Purif. Technol.* **2018**, *207*, 206.
124. H. Sopha, L. Hromadko, M. Motola, J. M. Macak, *Electrochem. commun.* **2020**, *111*, 106669.
125. H. Sopha, A. Kashimbetova, L. Hromadko, I. Saldan, L. Celko, E. B. Montufar, J. M. Macak, *Nano Lett*. **2021**, *21*, 8701.
126. H. Sopha, A. Kashimbetova, M. Baudys, P. K. Chennam, M. Sepúlveda, J. Rusek, E. Kolibalova, L. Celko, E. B. Montufar, J. Krysa, J. M. Macak, *Nano Lett*. **2023**, *23*, 6406.
127. H. Asoh, M. Ishino, H. Hashimoto, *RSC Adv*. **2016**, *6*, 90318.
128. H. Asoh, M. Ishino, H. Hashimoto, *J. Electrochem. Soc.* **2018**, *165*, C295.
129. H. Asoh, S. Miura, H. Hashimoto, *ACS Appl. Nano Mater*. **2019**, *2*, 1791.
130. J. P. Guerrette, S. M. Oja, B. Zhang, *Anal. Chem.* **2012**, *84*, 1609.
131. M. Ongaro, A. Gambirasi, P. Ugo, *ChemElectroChem* **2016**, *3*, 450.
132. H. Sopha, J. Rodriguez-Pereira, V. Cicmancova, J. M. Macak, *ChemElectroChem* **2021**, *8*, 3827.
133. S. Chen, Y. Ni, J. Zhang, Y. Dan, W. Zhang, Y. Song, X. Zhu, *Electrochem. commun.* **2021**, *125*, 106991.
134. D. Xu, X. Feng, Y. Song, X. Li, J. Zhang, S. Chen, X. Shen, *Electrochem. commun.* **2020**, *119*, 106822.
135. J. Polivka, *High Freq. Electron.* **2007**, *1*, 32.
136. B. D. Wiltshire, M. H. Zarifi, *Sensors Actuators B Chem*. **2021**, *341*, 130014.
137. O. Korostynska, A. Mason, A. Al-Shamma'a, *Sens. Rev.* **2014**, *34*, 182.
138. E. Monroy, F. Omn s, F. Calle, *Semicond. Sci. Technol.* **2003**, *18*, R33.
139. Y. Zou, Y. Zhang, Y. Hu, H. Gu, *Sensors* **2018**, *18*, 2072.
140. S. Yang, J. Gong, Y. Deng, *J. Mater. Chem.* **2012**, *22*, 13899.
141. Y. Ke, X. Wang, *J. Invest. Dermatol.* **2021**, *141*, 1104.
142. D. Stoll, J. Danforth, K. Zhang, A. Beck, *J. Chromatogr. B* **2016**, *1032*, 51.
143. G. Gruber, J.-L. Bertrand-Krajewski, J. De Beneditis, M. Hochedlinger, W. Lettl, *Water Pract. Technol.* **2006**, *1*, wpt2006020.
144. H. Kind, H. Yan, B. Messer, M. Law, P. Yang, *Adv. Mater.* **2002**, *14*, 158.
145. M. H. Zarifi, A. Mohammadpour, S. Farsinezhad, B. D. Wiltshire, M. Nosrati, A. M. Askar, M. Daneshmand, K. Shankar, *J. Phys. Chem. C* **2015**, *119*, 14358.

146. N. Mahdi, R. Kisslinger, H. Sharma, M. H. Zarifi, M. Daneshmand, K. Shankar, *2016 IEEE SENSORS*, Orlando, FL, USA, **2016**, pp. 1–3. https://doi.org/10.1109/ICSENS.2016.7808782
147. M. H. Zarifi, B. Wiltshire, N. Mahdi, P. Kar, K. Shankar, M. Daneshmand, *Nanoscale* **2018**, *10*, 4882.
148. B. D. Wiltshire, M. Alijani, S. Mohammadi, A. Hosseini, J. M. Macak, M. H. Zarifi, *ACS Appl. Mater. Interfaces* **2022**, *14*, 6203.
149. M. H. Zarifi, B. D. Wiltshire, N. Mahdi, K. Shankar, M. Daneshmand, *ACS Appl. Mater. Interfaces* **2018**, *10*, 29857.
150. M. Alijani, B. D. Wiltshire, H. Sopha, Z. Sarpanah, J. Mistrik, L. Hromadko, M. H. Zarifi, J. M. Macak, *Appl. Mater. Today* **2023**, *32*, 101832.
151. M. C. Jain, M. Alijani, B. D. Wiltshire, J. M. Macak, M. H. Zarifi, In *2022 IEEE/MTT-S Int. Microw. Symp.—IMS 2022*, Denver, CO, USA, **2022**, pp. 133–136. https://doi.org/10.1109/IMS37962.2022.9865511
152. S. V. Kireev, S. L. Shnyrev, *Laser Phys.* **2015**, *25*, 075602.
153. B. D. Wiltshire, M. Alijani, H. Sopha, D. Pavliňák, L. Hromadko, R. Zazpe, S. M. Thalluri, E. Kolibalova, J. M. Macak, M. H. Zarifi, *ACS Appl. Mater. Interfaces* **2023**, *15*, 18379.
154. M. H. Zarifi, S. Farsinezhad, K. Shankar, M. Daneshmand, *IEEE Microw. Wirel. Components Lett.* **2015**, *25*, 621.
155. J. M. Macak, M. Zlamal, J. Krysa, P. Schmuki, *Small* **2007**, *3*, 300.
156. H. Sopha, M. Baudys, M. Krbal, R. Zazpe, J. Prikryl, J. Krysa, J. M. Macak, *Electrochem. commun.* **2018**, *97*, 91.
157. J. Lincho, J. Gomes, M. Kobylanski, B. Bajorowicz, A. Zaleska-Medynska, R. C. Martins, *Process Saf. Environ. Prot.* **2021**, *152*, 601.
158. M. Motola, M. Baudys, R. Zazpe, M. Krbal, J. Michalička, J. Rodriguez-Pereira, D. Pavliňák, J. Přikryl, L. Hromádko, H. Sopha, J. Krýsa, J. M. Macak, *Nanoscale* **2019**, *11*, 23126.
159. H. Sopha, M. Baudys, L. Hromadko, M. Lhotka, D. Pavlinak, J. Krysa, J. M. Macak, *Appl. Mater. Today* **2022**, *29*, 101567.
160. R. Montenegro-Ayo, J. C. Morales-Gomero, H. Alarcon, A. Corzo, P. Westerhoff, S. Garcia-Segura, *Chemosphere* **2021**, *268*, 129320.
161. S. Franz, D. Perego, O. Marchese, M. Bestetti, *J. Water Chem. Technol.* **2015**, *37*, 108.
162. H. Kim, D. Kim, W. Kim, Y.-C. Ha, S.-J. Sim, S. Kim, W. Choi, *Appl. Catal. A Gen.* **2016**, *521*, 174.
163. J. P. Ghosh, G. Achari, C. H. Langford, *Water Environ. Res.* **2016**, *88*, 785.
164. C. Xiang, L. Sun, Y. Wang, G. Wang, X. Zhao, S. Zhang, *J. Phys. Chem. C* **2017**, *121*, 15448.
165. E. Mena, M. J. Martín de Vidales, S. Mesones, J. Marugán, *Catal. Today* **2018**, *313*, 33.
166. J. S. Khaw, M. Curioni, P. Skeldon, C. R. Bowen, S. H. Cartmell, *J. Nanotechnol.* **2019**, *2019*, 5902346.
167. R. Narayanan, T.-Y. Kwon, K.-H. Kim, *Mater. Lett.* **2009**, *63*, 2003.
168. R. Narayanan, T. Y. Kwon, K. H. Kim, *Mater. Chem. Phys.* **2009**, *117*, 460.
169. P. M. Perillo, D. F. Rodriguez, *Nanosci. Methods* **2012**, *1*, 194.
170. A. G. Kontos, A. Katsanaki, T. Maggos, V. Likodimos, A. Ghicov, D. Kim, J. Kunze, C. Vasilakos, P. Schmuki, P. Falaras, *Chem. Phys. Lett.* **2010**, *490*, 58.
171. A. G. Kontos, A. Katsanaki, V. Likodimos, T. Maggos, D. Kim, C. Vasilakos, D. D. Dionysiou, P. Schmuki, P. Falaras, *Chem. Eng. J.* **2012**, *179*, 151.

How to cite this article: H. Sopha, M. Alijani, M. Sepúlveda, J. M. Macak, *Nano Select* **2024**, *5*, 2300140. https://doi.org/10.1002/nano.202300140

AUTHOR BIOGRAPHIES

Hanna Sopha received her PhD degree in analytical chemistry from the University of Ljubljana (Slovenia) in 2013. Afterwards she joined the University of Pardubice (Czech Republic) as a postdoctoral research fellow in the field of electroanalytical chemistry. Since 2015, she has been working as senior scientist at the Centre of Materials and Nanotechnologies of the same university. Her research is focused on the anodization of valve metals towards novel nanotubular and nanoporous structures, as well as application and functionalization of these structures.

Mahnaz Alijani received her BSc and MSc degrees in material engineering in Iran. She completed her PhD in advanced materials at the Central European Institute of Technology (CEITEC) in the Czech Republic in 2023. Presently, she serves as a postdoctoral researcher at CEITEC. Since 2013, her research has centered on TiO_2 nanomaterials, with a dedicated focus on TiO_2 nanotube layers since 2019. Her current endeavors revolve around developing high aspect ratio TiO_2 nanotube layers with surface modifications for applications in sensing and biosensing.

Marcela Sepúlveda received her PhD degree in materials engineering from the University of Antioquia (Colombia) in 2019. From 2019 to 2021 she worked at the Central European Institute of Technology (CEITEC-VUT, Czech Republic) as a postdoctoral research fellow, being involved in the anodization of valve metal bilayers towards nanocolumnar structures. In 2021, she joined the Centre of Materials and Nanotechnologies of the University of Pardubice (Czech Republic) as a junior researcher. Her research is focused on the anodization of valve metals and their alloys, and the modification and application of the resulting nanostructures.

Jan M. Macak received his PhD in materials science in 2008 at Friedrich-Alexander University of Erlangen-Nürnberg (Germany) based on his thesis devoted to the preparation of TiO_2 nanotubes by titanium anodization. Then he worked for 3 years in the private sector. In 2012 he joined the University of Pardubice. Since 2015, Dr. Macak has been working as a senior researcher at the Centre for Materials and Nanotechnologies (CEMNAT) of the Faculty of Chemical Technology. From 2018 he has been a group leader and senior researcher at the Central European Institute of Technology (CEITEC) of the Brno University of Technology. His research interest lies in the development of low-dimensional nanostructures (such as nanotubes, nanolayers, nanofibers) using various methods, necessary characterization and also utilization in various applications, for example, in solar cells, catalysts, batteries, and so on, together with cooperating partners. For his outstanding scientific achievements, and in recognition of his scientific research work, he received several prestigious awards, including Neuron Award 2015 for outstanding achievements of young scientist in the field of chemistry, and the TechConnect Award 2019 for innovation. He has been granted ERC Starting Grant in 2015. He serves as the editor of the Frontiers of Nanotechnology and from 2024 will become Chairman of the European Section of the Electrochemical Society.